# Improving membrane distillation performance: morphology optimization of hollow fiber membranes with selected non-solvent in dope solution

Minwei Yao[a], Jiawei Ren[a], Nawshad Akther[a], Yun Chul Woo[b], Leonard D. Tijing[a], Seung-Hyun Kim[c], Ho Kyong Shon[a],*

[a] Centre for Technology in Water and Wastewater, School of Civil and Environmental Engineering, University of Technology Sydney (UTS), P. O. Box 123, 15 Broadway, NSW 2007, Australia

[b] Department of Land, Water, and Environment Research, Korea Institute of Civil Engineering and Building Technology (KICT), 283 Goyang-Daero, Ilsanseo-Gu, Goyang-Si, Gyeonggi-Do, 10223, Republic of Korea

[c]Civil Engineering Department, Kyungnam University, Wolyoung-dong, Changwon, 631-701, Republic of Korea

*Corresponding authors: H.K. Shon, e-mail: Hokyong.Shon-1@uts.edu.au, Tel: +61 2 9514 2629

**Keywords:** hollow fiber membrane; membrane distillation; NIPS; morphology; non-solvent; crystallinity

**Abstract**

This study aimed at improving membrane distillation (MD) performance by mixing various non-solvents (NSs) in polymer dope solutions. The effect of each NS on the inner structure and surface morphology of hollow fiber (HF) membrane was investigated. Membrane morphology is manipulated by controlling liquid-liquid (L-L) and solid-liquid (S-L) demixing time, which is a function of the viscosity and water affinity of dope solutions. Consequently, the addition of NSs altered membrane morphology by affecting the diffusion rate during NS induced phase separation (NIPS) process. The performance results showed that the dope solution composed of 11/71.2/17.8 wt.% polyvinylidene fluoride (PVDF)/ triethyl phosphate (TEP)/toluene produced the most promising HF membrane for MD. The optimal membrane demonstrated a unique bicontinuous structure with increased porosity and mean pore size. The addition of toluene as NS in dope solutions enhanced crystallization process, which increased the Young's modulus of membrane but slightly decreased its maximum tensile strength at break. The optimal PVDF HF membrane demonstrated a steady flux of 18.9 LMH at 60 °C/20 °C of feed/permeate temperatures and a salt rejection of 99.99 % when tested for 72 h. The results suggest that incorporation of toluene as a NS into PVDF dope solutions can increase permeation performance in MD by enhancing the morphology of HF membranes.

## 1. Introduction

Membrane distillation (MD) is widely considered as one of the most promising next-generation membrane technologies as its unique mechanism demonstrates strong capacities in desalination and wastewater treatment applications where traditional membrane technologies are impractical (Deshmukh et al., 2018; McGaughey, Gustafson, & Childress, 2017). However, MD has not been fully commercialized yet due to several major drawbacks; one of them is its relatively low permeation performance, which makes this energy-intensive process even less competitive (Eykens, De Sitter, Dotremont, Pinoy, & Van der Bruggen, 2017).

Lack of ideally designed membranes for MD is a major reason for the low permeation performance (Y. Li, Dong, & Zhu, 2018). Although many studies have been conducted to develop MD membranes with higher permeation, the fabrication cost of these membranes is very high making them unviable for industrial upscaling (H. Zhang, Li, Sun, Miao, & Gu, 2018; Zhu, Jiang, & Matsuura, 2015). Therefore, a simple and effective approach is needed to develop high-performance MD membranes. An ideal MD membrane should have a highly hydrophobic surface, narrow pore size distribution and large porosity to achieve high permeation flux (Qiu, Peng, Ge, Villacorta Hernandez, & Zhu, 2018; Shi, Ma, Ma, Wang, & Sun, 2012). In regards to the effect of heat loss in MD, it is also essential to optimize the membrane thickness to balance the trade-off between the flux performance and thermal efficiency (Wang, Teoh, & Chung, 2011).

Polyvinylidene fluoride (PVDF) is favored as the base material for MD membranes due to its low thermal conductivity, high chemical resistance and mechanical strength (García-Payo, Essalhi, & Khayet, 2010; Venault, Chang, Wu, & Wang, 2014). Unlike other non-reactive hydrophobic polymers, PVDF can be used to fabricate cost-effective membranes as it can be easily dissolved in various common solvents. Therefore, multiple fabrication approaches have been implemented using PVDF as dope solutions (Tao, Liu, Ma, & Xue, 2013). Electrospinning is one of the fabrication methods that has been extensively employed to develop nanofibrous PVDF membranes with high permeation flux, but they are prone to rapid pore wetting owing to low liquid entry pressure (LEP) (Liao, Wang, Tian, Qiu,

& Fane, 2013). Moreover, electrospinning membranes are not practical for large-scale manufacturing (Ahmed, Lalia, & Hashaikeh, 2015).

Non-solvent induced phase separation (NIPS) process has also been comprehensively studied for MD membrane development. The PVDF MD membranes made via NIPS method generally have a smaller mean pore size and porosity than the nanofibrous membranes prepared using the same dope solution; thus, demonstrating lower permeation flux in MD (Buonomenna, Macchi, Davoli, & Drioli, 2007; Munirasu, Banat, Durrani, & Haija, 2017). In general, the NIPS PVDF membranes have finger-like macrovoids underneath their thick skin layers, and dense sponge structure for bottom layers (Bonyadi & Chung, 2009; Pinnau & Koros, 1993). It has been reported that membranes with macrovoids have multiple disadvantages like high sensitivity to wetting, high tendency towards scaling and intra-pore salt precipitation, which lower membrane stability in long-term MD operation (Hung, Wang, Lai, & Chou, 2016). Besides electrospinning and NIPS, thermally induced phase separation (TIPS) method has also been employed for MD membrane fabrication. Jung et al. (2018) found that hollow fiber (HF) membranes with macrovoid-free bicontinuous structure can be developed using TIPS method and proper diluent ratio as it allowed both liquid-liquid (L-L) and solid-liquid (S-L) demixing to occur at the right time (Jung et al., 2018). However, TIPS is not a cost-effective method due to its technical limitations (e.g., high heat energy consumption) (Sukitpaneenit & Chung, 2009).

It is more cost-effective and practical to obtain high-performance MD membranes by improving the NIPS approach. Hence, several studies considered the development of strategies to deal with the issues of NIPS membranes (large macrovoids and small pore size). To prepare NIPS PVDF membranes without macrovoids, the main strategy is to delay L-L demixing rates (Smolders, Reuvers, Boom, & Wienk, 1992). Various techniques have been employed to delay L-L demixing rates, such as increasing polymer concentrations or molecular weight, using weak coagulants, exposing casting dope solutions to water vapor before immersion into coagulation bath, and decreasing coagulant bath temperatures (Buonomenna et al., 2007; Munirasu et al., 2017; P.-Y. Zhang et al., 2013). However, these techniques either sacrifice membrane porosity or hinder large-scale production due to high economic and environmental costs. Recently, Nejati et al. (2015) and Chang et al. (2017) reported that L-L demixing

rates could be greatly decreased by using triethyl phosphate (TEP) as polymer solvent owing to its higher viscosity and lower affinity with water (Nejati, Boo, Osuji, & Elimelech, 2015; Yeow, Liu, & Li, 2003). Hence, it is possible to fabricate macrovoid-free membranes without using costly approaches. Although membranes prepared using TEP as a polymer solvent have demonstrated better MD performance in both short and long-term operations, their improvement is limited due to relatively dense skin layers and small surface porosity. These characteristics are common among PVDF membranes prepared using NIPS method with water as a coagulant (Abed, Kumbharkar, Groth, & Li, 2012; Chang, Zuo, Zhang, O'Brien, & Chung, 2017). Therefore, further improvement in the inner structure and surface morphology of NIPS HF membranes is required to improve permeation performance in MD processes.

In this paper, membranes with improved MD performance were developed by determining the effects of various non-solvents (NSs) in polymer dope solutions on the inner structure and surface morphology of the membranes. The viscosity and water affinity of the dope solutions were controlled to manipulate the sequence of L-L and S-L demixing rates during the NIPS process to change the membrane morphology. The permeation performance of HF membranes in MD was evaluated based on the improvement in membrane morphology and mean pore size. The results indicate that the optimization of polymer, solvent, and NS compositions in dope solutions is essential to design high-performance membranes for MD processes.

## 2. Materials and methods

### 2.1 Materials

High molecular weight PVDF polymer pellets (Kynar® HSV900) were kindly provided by Arkema Inc. Triethyl phosphate (TEP, 99%), N-methyl-2-pyrrolidone (NMP, 99.5%), ethanol (100%), acetone (99.5%) and dibutyl phthalate (DBP, >97%) were all purchased from Chem-Supply. Toluene (≥99.5%) and sodium chloride (NaCl) were bought from Sigma-Aldrich and Ajax Finechem, respectively. Tap water was used as a coagulant in spinning processes. Distilled water was used as permeate. All chemicals were used as received.

### 2.2 Determination of dope solution recipes

In NIPS approaches, the sequence of L-L demixing and S-L demixing strongly affects membrane morphology (Lin, Chang, Chen, & Cheng, 2002). In general, S-L demixing (crystallization) takes a much slower pace than L-L demixing. If L-L demixing occurs at a very fast rate during NIPS processes, macrovoid structures are formed underneath the skin layer of the membrane and the remaining layers are dominated by sponge-like structures (cellular pores). On the other hand, if L-L demixing lags behind S-L demixing process, then large spherulitic crystal structures become dominant. Viscosity and water affinity of PVDF dope solutions can strongly influence NIPS demixing processes; hence, they are chosen to optimize membrane morphology. Water affinity is determined by Hansen solubility (dipole force) of liquid chemicals. Generally, increasing solution viscosity or decreasing water affinity leads to a delayed L-L demixing and promotes S-L demixing in NIPS process, so spherulitic crystal structures become dominant (Chang et al., 2017; Mansourizadeh & Ismail, 2011; Smolders et al., 1992). Therefore, in this study, high molecular weight PVDF was chosen for all recipes as its dope solution has high viscosity even at low concentration. Triethyl phosphate (TEP) was used as a solvent due to its low water affinity and good compatibility with PVDF.

To manipulate demixing rates in phase inversion, NSs with various combination of viscosity and Hansen solubility (water affinity) were selected. In addition, the selected NSs must comply with the following requirements:

(i.) forms a homogenous polymer solution at 80 °C after mixing with NS and remains stable for at least 10 h once the dope solution cools down to room temperature
(ii.) provides suitable dope solution viscosity for HF membrane fabrication
(iii.) has low toxicity and causticity; less harmful to the human and ecological system
(iv.) cost-effective

After careful consideration, toluene, acetone and DBP were used as NSs for preparation of dope solutions. The main properties of the chemicals used in this study are listed in Table 1.

**Table 1.** Hansen solubility parameters at 25 °C, molecular weight, density, partition coefficient, and viscosity of various chemicals used in this study.

| **Materials** | **Viscosity (cP)** | **Hansen solubility, $\delta_p$ $(J.cm^{-3})^{1/2}$** | **Molecular weight ($g.mol^{-1}$)** | **Density ($g.\ cm^{-3}$)** | **Partition coefficient, log Kow** |
|---|---|---|---|---|---|
| PVDF (HSV 900) | N/A | 12.1 | N/A | 1.78 | N/A |
| Water | 0.89 | 16 | 18 | 1 | - |
| N-Methyl-2-pyrrolidone (NMP) | 1.65 | 12.3 | 99 | 1.03 | -0.38 |
| Triethyl phosphate (TEP) | 1.46 | 11.5 | 182 | 1.07 | 0.8 |
| Toluene* | 0.56 | 1.4 | 92 | 0.87 | 2.73 |

| | | | | | |
|---|---|---|---|---|---|
| Acetone* | 0.31 | 10.4 | 58 | 0.78 | -0.24 |
| Dibutyl phthalate (DBP)* | 19.6 | 8.6 | 278 | 1.05 | 4.5 |

*NSs used in this study

## 2.3 Preparation of dope solution and fabrication of PVDF hollow fiber membranes

PVDF was used as a base polymer in this study. Homogenous polymer dope solutions were prepared by dissolving PVDF powder (11 wt.%) in a mixture of TEP and NS at 80 °C under continuous stirring for 72 h. The various combinations of TEP and NS used to prepare dope solutions, and the names of corresponding HF membranes are listed in Table 2. A control sample, NMP0, was prepared using NMP instead of TEP as a solvent. The prepared dope solutions were then poured into the syringe pump (Model 500D, Teledyne Isco, USA) and left to degas at room temperature for 24 h before HF membrane fabrication.

**Table 2.** Naming convention and dope solution compositions of hollow fiber membranes developed in this study.

| Sample | NS chemical | Dope concentration (wt.%) | | | |
|---|---|---|---|---|---|
| | | PVDF | NMP | TEP | NS |
| NMP0 | - | 11 | 89.0 | - | - |
| TEP0 | - | | - | 89.0 | - |
| TEPA-1 | Acetone | | - | 80.1 | 8.9 |
| TEPA-2 | Acetone | | - | 71.2 | 17.8 |
| TEPD-1 | DBP | | - | 80.1 | 8.9 |
| TEPD-2 | DBP | | - | 71.2 | 17.8 |
| TEPT-1 | Toluene | | - | 80.1 | 8.9 |
| TEPT-2 | Toluene | | - | 71.2 | 17.8 |

All HF membranes were fabricated using a dry-jet wet spinning process. Table 3 lists the detailed spinning parameters used in this study, which were kept constant for the fabrication of all HF membranes. The as-spun HF membranes were stored in a distilled water tank for three days after the phase inversion process. The water in the storage tank was changed daily to remove residual chemicals from the membranes completely. After three days, the HF membranes were dried at room temperature.

**Table 3.** PVDF hollow fiber spinning conditions

| Parameter | Value |
|---|---|
| Dope extrusion rate (mL/min) | 5.0 |
| Bore fluid flow rate (mL/min) | 1.9 |

| | |
|---|---|
| External coagulant and bore fluid | Tap water |
| Air gap (cm) | 2 |
| Dope solution temperature (°C) | 25 |
| Coagulant bath and spinneret temperature (°C) | 25 |

Ten fibers of each PVDF HF membrane fabricated with various dope solutions were used to make a module with a total surface area of 82 $cm^2$. The internal diameter of this membrane module was 8 mm.

## 2.4 Characterizations

### 2.4.1 PVDF dope solution viscosity

The viscosity of PVDF dope solutions was measured at room temperature using a dial viscometer with spindle #4 (LVT, Brookfield, USA). Readings were taken after full stabilization was achieved. The solution viscosity was interpreted from a table provided by the manufacturer.

### 2.4.2 Membrane morphology

The surface morphology and inner structure of HF membrane samples were examined by a scanning electron microscope (SEM, Zeiss Supra 55VP), which was operated at 10 kV. The samples were freeze-fractured using liquid nitrogen for cross-section study. All the samples were sputter coated with a 15 nm-thick gold/palladium layer before analysis. Membrane samples were randomly selected to evaluate the diameters, thickness and inner structures of the membranes.

Membrane surface roughness was measured using atomic force microscopy (AFM, Dimension 3100 Scanning Probe Microscope, Bruker) in tapping mode. A scanning area of 10.0 μm x 10.0 μm was used for all membrane samples. Each sample was scanned three times at randomly chosen locations to obtain the average root mean square roughness ($R_q$).

### 2.4.3 Contact angle, porosity and pore size measurement

Contact angle measurements were made using an optical tensiometer (Attension Theta Lite 100, Biolin Scientific) to evaluate membrane surface hydrophobicity. The contact angles were reported as the average of 5 random measurements made for each sample.

Membrane porosity was determined using the gravimetric method as reported previously (Yao et al., 2016). The weight ($w_1$, g) of the wet membrane sample was obtained by completely immersing it in ethanol. The wet membrane sample was then fully dried to measure its dry weight ($w_2$, g). The porosity of HF membrane samples was calculated using Eq. 1,

$$\varepsilon_m = \frac{(w_1 - w_2)/\rho_e}{\frac{w_1 - w_2}{\rho_e} + w_2/\rho_{PVDF}} \quad (1)$$

where $\rho_e$ and $\rho_{PVDF}$ is the density of ethanol and PVDF, respectively ($g/cm^3$).

The mean pore size of HF membrane samples was measured using a PMI liquid-liquid permeameter (LLP-1100A, Porous Materials, Inc.) with a resolution of 1 in 60,000 and a flow resolution of 0.0001 cc/min. Isobutanol was used as the fluid to measure the mean pore size. For each HF membrane sample, the average of three measurements was used as its mean pore size.

### 2.4.4 Crystallinity and mechanical strength

Differential scanning calorimetry (DSC) was conducted using DSC 2000 (TA Instruments) to measure the heat flow of polymer samples during the melting process. Crystallinity was calculated based on obtained enthalpy. Average of three measurements were reported for each sample.

The mechanical properties of HF membrane samples were measured by a bench-type material tester (Lloyd Instruments, Ametek) with a starting gauge length of 25 mm and a stretching rate of 50 mm/min. The average values were obtained from five tests conducted for each sample.

## 2.5 Membrane distillation configuration

A direct contact MD (DCMD) configuration was set up to evaluate the performance of membrane modules operating at outside-in mode. A 7 wt.% NaCl solution, which was heated to 60 °C, was used as feed solution for DCMD tests; whereas, distilled water maintained at 20 °C was used as permeate. The flow rates of both feed and permeate were 300 mL/min. The permeation flux and salt rejection were obtained using Eq. 2 and 3, respectively

$$Flux\ (LMH) = \frac{\Delta W}{\rho_w \times A \times t} \tag{2}$$

$$Rejection\ (\%) = \left(1 - \frac{C_p}{C_f}\right) \times 100 \tag{3}$$

where ΔW (kg) is the increase in permeate weight during measuring period t (h), $\rho_w$ (kg/ L) is the density of pure water (assuming permeate is pure water), A ($m^2$) is the effective membrane area, $C_p$ and $C_f$ are the concentrations of NaCl in permeate and feed, respectively.

Commercial HF membranes provided by Econity were tested in DCMD configuration for comparison with fabricated membranes. The commercial membrane had an inside and outside diameter of 0.77 mm and 1.3 mm, respectively. The porosity and mean pore size of the commercial membrane was 0.1 μm and 63%, respectively.

## 3. Results and discussion

### 3.1 Effect of various NS on the inner structure of hollow fiber membranes

The inner structures of HF membranes were determined by dope solutions which can be adjusted by changing the solvent and NS. Fig. 1(a-c) shows that the HF membrane prepared using NMP as the solvent (NMP0) consisted of an asymmetric inner structure with large macrovoids underneath the thick skin layer and dense sponge structure in the bottom layer. On the other hand, the macrovoid formation was prevented when TEP was used as the dope solution solvent. Fig. 1(d-f) illustrates the morphology of TEP0, which has a macrovoid-free fibrous structure at the shell and spherulitic structures with large open pores at the lumen. Nejati et al. obtained a flat sheet membrane with a similar asymmetric morphology using TEP as a dope solvent. They suggested that initial L-L demixing created a less permeable wall to NS diffusion which delayed the demixing in sublayers and led to the formation of spherulitic structures at the bottom layers (Nejati et al., 2015).

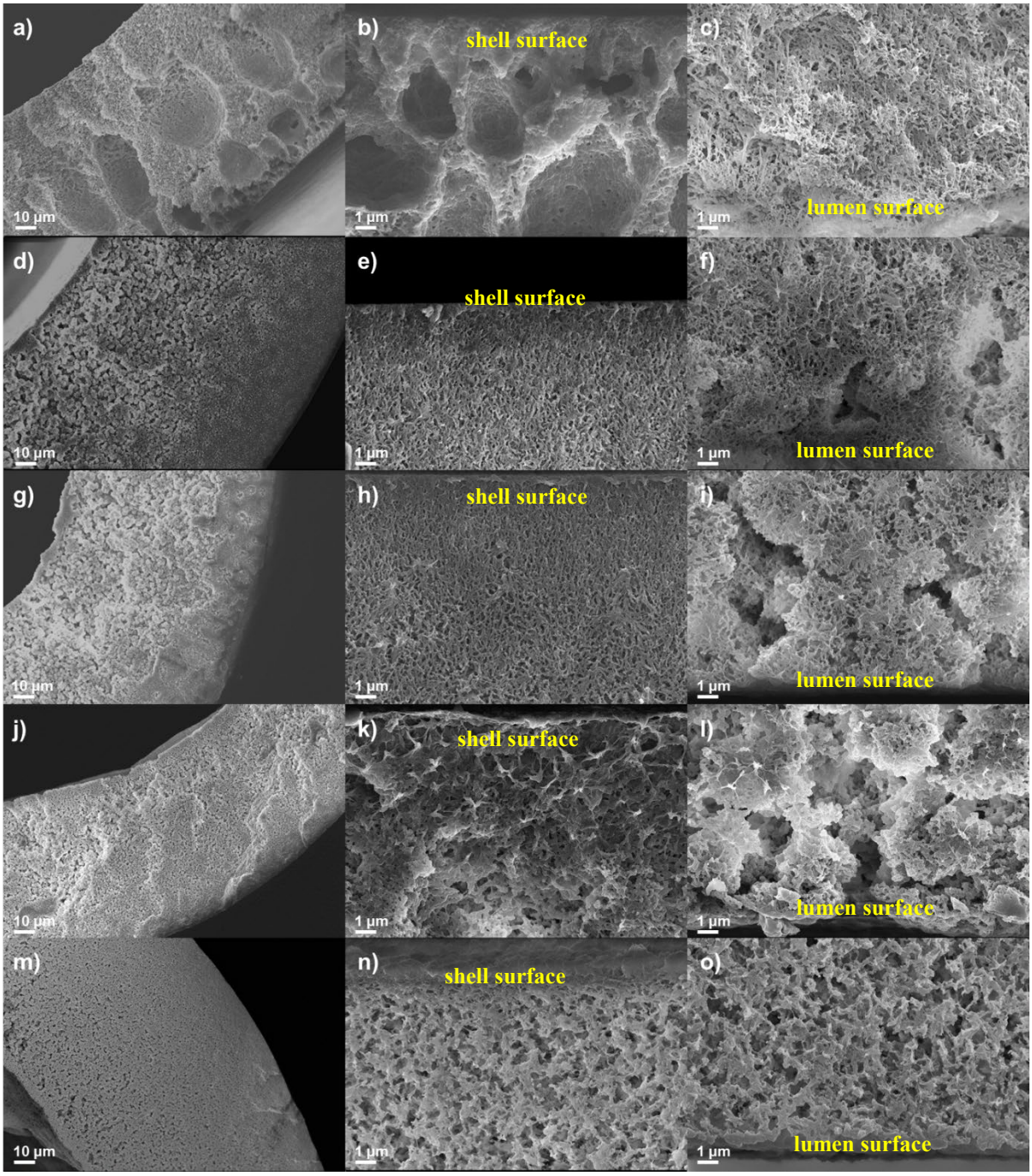


**Fig. 1.** SEM images displaying the cross-section of hollow fiber membranes cast from 11 wt.% PVDF in (a-c) NMP; (d-f) TEP; (g-i) TEP and 17.8 wt.% acetone; (j-l) TEP and 17.8 wt.% DBP; and (m-o) TEP and 17.8 wt.% toluene.

The optimization of HF membrane inner structures is expected to improve MD permeation performance, which can be achieved by manipulating the viscosity and water affinity of polymer solutions by incorporating various NS like acetone, DBP and toluene into the dope solution. Acetone has a much lower viscosity than TEP, so the addition of 20 wt.% acetone into polymer solution reduced the dope solution viscosity from 332 to 278 P. In addition to the decreased viscosity, the polymer solution

containing acetone has higher water affinity because of the low partition coefficient of acetone. Therefore, a faster L-L demixing occurred in the HF membrane prepared using acetone-containing dope solution that resulted in TEPA-2 having a different morphology than the TEP0. TEPA-2 (Fig. 1i) shared similar membrane inner structure with that of TEP0 (Fig. 1f), which is dominant with large spherulitic crystal structures at the lumen side of the HF membrane; however, it had a denser and thicker layer comprising of fibrous structures at the shell side. Moreover, with decreased membrane thickness, the inner diameter of TEPA-2 was larger than TEP0 due to promoted L-L demixing (Table 4), which is consistent with a previous study (Chang et al., 2017). In general, a membrane fabricated with faster L-L demixing has thinner membrane thickness. However, the improvement in MD performance using TEPA-1 and TEPA-2 were not expected as the benefits of a decrease in membrane thickness can be offset by the potential decrease in the porosity and pore size due to the morphological changes.

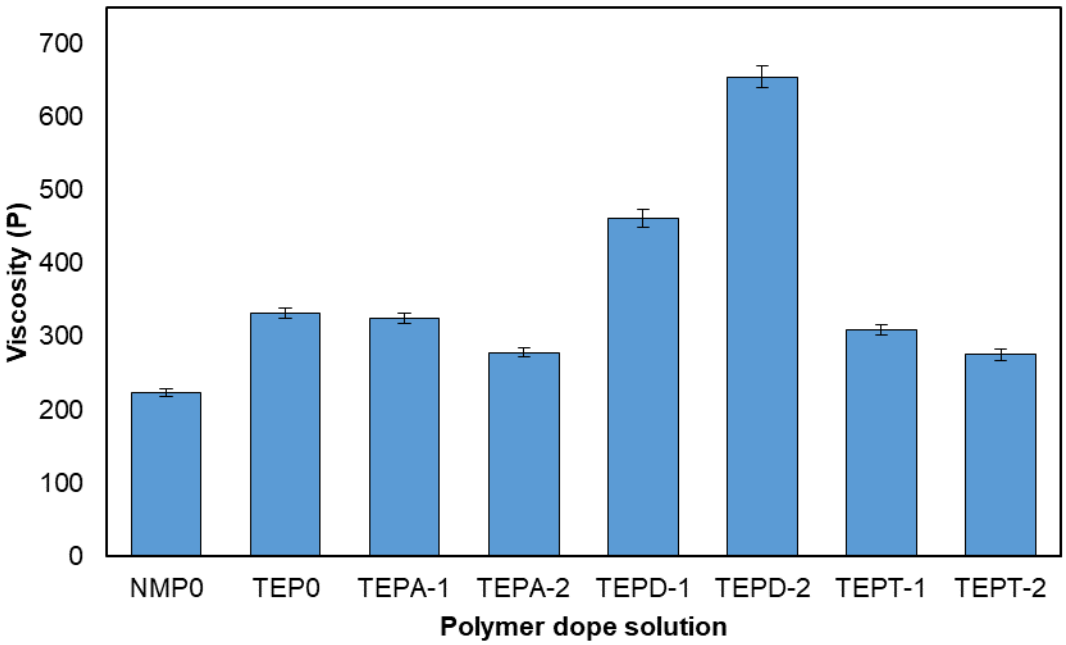


**Fig. 2.** The viscosity of various polymer dope solutions.

The addition of DBP as NS into polymer solutions led to a significantly different HF membrane structure from that of TEP0 and TEPA-2. The dope solution incorporated with DBP has a significantly higher viscosity (Fig. 2) and lower water affinity (Table 1); thereby, leading to a greatly promoted S-L demixing (crystallization). Fig. 1 (j-l) shows that TEPD-2 is composed of large spherulitic crystal nodes with large open pores that are dominant at the shell side unlike TEP0 and TEPA-2. The spherulitic structures were also observed by Sukipaneenit and Chung when weak coagulant (e.g., ethanol) was used in coagulation bath as L-L demixing rate was greatly reduced and crystallization became dominant

(Sukitpaneenit & Chung, 2009). A membrane containing large open pores is likely to have a low LEP and is prone to wetting in MD.

On the other hand, HF membranes fabricated with polymer dope solutions containing toluene produced very distinct structures. The polymer solution of TEPT-2 had a reduced viscosity of 275 P and reduced water affinity owing to its low partition coefficient. As such, the usage of the dope solution containing toluene led to a unique NIPS process that resulted in the formation of symmetric inner structures as can be seen in Fig. 1(m-o), while other HF membranes had asymmetric structures. The large spherulitic crystal structures with open pores, as can be found in TEP0, TEPA-2 and TEPD-2, were not observed in TEPT-2. These HF membranes confirmed a uniform bicontinuous structure comprising of interlinked small spherulitic crystal structures, which had pores with the same size throughout the membranes. The absence of large spherulitic crystal structures with open pores at the lumen side (Fig. 1l) occurred due to the presence of toluene in dope solutions. For comparison, TEPA-2 having lower dope viscosity, had large spherulitic crystal structures at lumen side. It is assumed that the combination of both decreased water affinity and viscosity would contribute to a balance between L-L demixing and S-L demixing, which would promote the diffusion of dope solution into coagulants without fast solidification. Therefore, all portions of the dope solution have the same diffusion and solidification rates, which results in the formation of those bicontinuous structures. Our work is the first to successfully fabricate HF membranes with macrovoid-free bicontinuous inner morphology via NIPS without using weak coagulants.

### 3.2 Porosity and pore size distribution

Membrane pore structures determine the porosity and pore size distribution as a result of NIPS process, which can be manipulated by adjusting the viscosity and water affinity of polymer dope solutions (García-Payo et al., 2010; Q. Li, Xu, & Yu, 2010; Tao et al., 2013). Table 4 shows the porosity and pore size distribution of HF membranes fabricated with various dope solutions. Owing to its fastest L-L demixing rate, NMP0 possessed the lowest porosity and smallest mean pore size among all the samples despite the formation of macrovoids. On the other hand, HF membranes fabricated using dope solution with TEP solvent showed higher porosity. It is because higher viscosity and lower water affinity of dope solutions led to the formation of spherulitic crystal structures by slow S-L demixing (Ahmad, Otitoju, & Ooi, 2018; Lin, Chang, Chen, Lee, & Cheng, 2006). Addition of acetone as NS reduced the viscosity and increased the water affinity of dope solutions, which resulted in the formation of fibrous structure layers at the shell side (Fig. 1h). Thus, TEPA-1 and TEPA-2 demonstrated reduced porosity and mean pore size. In contrast, TEPD-2 had the highest mean pore size among all samples due to its spherulitic crystal structures that resulted from the much delayed L-L demixing. On the other side, the addition of toluene into the polymer solution increased the porosity of HF membranes because

of its bicontinuous structures with open pores. These membranes also demonstrated higher porosity (86.2% for TEPT-2), which contributed to the improvement of mass transfer efficiency in MD.

**Table 4.** Comparison of porosity, mean pore size, thickness, and inner and outer diameters of hollow fiber membranes using various dope solutions

| Sample | Porosity (%) | Mean pore size (nm) | $\Phi_{outer}$ (µm) | $\Phi_{inner}$ (µm) | Thickness (µm) |
|---|---|---|---|---|---|
| NMP0 | 75.1 ± 0.9 | 26.3 ± 0.9 | 1072 ± 13 | 796 ± 15 | 138 ± 10 |
| TEP0 | 81.8 ± 1.0 | 47.7 ± 1.2 | 968 ± 16 | 618 ± 15 | 175 ± 12 |
| TEPA-1 | 80.5 ± 1.2 | 39.5 ± 1.1 | 978 ± 12 | 642 ± 15 | 168 ± 12 |
| TEPA-2 | 78.5 ± 1.2 | 026.3 ± 1.5 | 972 ± 12 | 662 ± 16 | 155 ± 9 |
| TEPD-1 | 81.6 ± 1.5 | 352.0 ± 2.1 | 966 ± 17 | 640 ± 21 | 163 ± 15 |
| TEPD-2 | 80.3 ± 1.7 | 424.2 ± 2.8 | 940 ± 25 | 650 ± 22 | 145 ± 12 |
| TEPT-1 | 83.2 ± 1.5 | 77.2 ± 2.0 | 1079 ± 12 | 719 ± 16 | 180 ± 14 |
| TEPT-2 | 86.2 ± 1.4 | 81.5 ± 1.9 | 1099 ± 14 | 719 ± 16 | 190 ± 13 |

The thickness of HF membranes varied although the same procedure was used to prepare all dope solutions and membranes. NMP0 had the lowest thickness among all samples owing to fast L-L demixing promoted by the low viscosity and high water affinity of its dope solution. Whereas, TEPT-2 experienced elevated diffusion of the dope solution in demixing processes causing it to be the thickest among all the samples.

### 3.3 Polymer crystallinity and mechanical strength

The degree of crystallinity in the PVDF membrane is dependent on the level of crystallization during the NIPS process, which can be critically affected by the addition of NSs into dope solutions. As a semi-crystalline polymer, PVDF can stay at either crystalline or amorphous state, and the demixing mechanism plays a critical role during the phase inversion. Fast L-L demixing of polymer solutions with strong NS usually forms PVDF at amorphous state (Wu, Jiang, & Hu, 2018). For this reason, NMP0 had the highest amount of PVDF polymer at amorphous state with the lowest crystallinity of 35% (Table 5). NMP0 also showed the highest tensile strength and strain at break among all the samples. Generally, a fast L-L demixing rate in polymer dope solution forms membranes with dense fibrous sponge structures, which have higher mechanical strength and lower crystallinity (P.-Y. Zhang et al., 2013). On the other hand, when L-L demixing is delayed during the phase inversion process, the inner structure of membranes will change from fibrous sponge structure to spherulitic crystal structure. Membranes with spherulitic crystal structures have low tensile strength and elongation at break; as such,

they are more fragile (Chang et al., 2017). Replacing NMP with TEP as a solvent in polymer solution led to delayed L-L demixing; therefore, the crystallinity of TEP0 greatly increased but its mechanical strength deteriorated.

TEPA-2 demonstrated improved tensile strength (from 2 to 2.2 MPa) and strain (from 0.57 to 0.62) while its crystallinity decreased, which was consistent with its increased proportion of fibrous structure (Fig. 1). The fibrous structures resulted from using acetone as an NS, which increased the L-L demixing rate by lowering the viscosity and increasing the water affinity of dope solutions. On the other hand, the addition of DBP into the dope solution formed membranes with large spherulitic crystal structures that resulted in high Young's modulus of 8.8 MPa and low elongation of 0.16. The high viscosity and low water affinity of DBP considerably hindered L-L demixing process, and S-L demixing became dominant in the phase inversion process. Hence, the crystallinity of TEPD-2 is also the highest (50%) among all tested samples. Bonyadi and Chung (2009) also found that delayed demixing increased Young's modulus of fabricated membranes. Any further decrease in the tensile strength and elongation at break of the HF membranes caused by phase inversion may damage the mechanical integrity.

The addition of toluene into the polymer solution exhibited similar effects to that of DBP on the HF membrane properties. Because of the slower L-L demixing rate, the crystallinities of TEPT-1 and TEPT-2 were slightly higher than those of TEP0 despite the lack of large spherulitic crystal structures. The membranes also had decreased tensile strengths and strains at break compared with TEP0, but they were much higher than those of the HF membranes prepared using a dope solution containing DBP as NS. This is because the distinct bicontinuous structures of these membranes were well interconnected with nodes as discussed in section 3.1. It can be concluded that TEPT-2 containing the bicontinuous inner structures with high mean pore sizes can still maintain mechanical integrity, which makes it suitable for MD applications.

**Table 5.** Comparison of mechanical strength and crystallinities of hollow fiber membranes using various dope solutions.

| Sample | Crystallinity (%) | Tensile strength at break (MPa) | Strain at break | Young's modulus (MPa) |
|---|---|---|---|---|
| NMP0 | 35.2 ± 1.3 | 2.83 ± 0.03 | 0.65 ± 0.03 | 4.35 ± 0.17 |
| TEP0 | 43.5 ± 2.0 | 2.04 ± 0.02 | 0.57 ± 0.05 | 3.60 ± 0.33 |
| TEPA-1 | 41.3 ± 1.6 | 2.17 ± 0.03 | 0.60 ± 0.05 | 3.63 ± 0.24 |
| TEPA-2 | 40.3 ± 0.6 | 2.28 ± 0.01 | 0.62 ± 0.03 | 3.68 ± 0.12 |
| TEPD-1 | 46.4 ± 2.2 | 1.92 ± 0.01 | 0.35 ± 0.01 | 5.51 ± 0.18 |
| TEPD-2 | 50.6 ± 2.1 | 1.45 ± 0.02 | 0.16 ± 0.01 | 9.07 ± 0.16 |
| TEPT-1 | 44.9 ± 1.5 | 1.95 ± 0.02 | 0.44 ± 0.02 | 4.43 ± 0.16 |

| | | | | |
|---|---|---|---|---|
| TEPT-2 | 46.6 ± 2.3 | 1.76 ± 0.01 | 0.32 ± 0.01 | 5.51 ± 0.15 |

### 3.4 Surface morphology, contact angle and surface roughness

Fig. 3 shows the surface morphology (shell skin) of HF membranes that are greatly affected by the phase inversion process. A slow L-L demixing usually results in delayed solidification of the surface layer, so the skin layer has larger surface pore sizes and rough surface. TEP0 (Fig. 3b) consisted of significantly larger surface pores than NMP0 (Fig. 3a). In general, the surface hydrophobicity is a function of surface roughness. Increasing surface roughness leads to higher surface hydrophobicity, which is represented by the contact angle of a water droplet (Franken, Nolten, Mulder, Bargeman, & Smolders, 1987). For NMP0, a fast L-L demixing process caused fast solidification of surface layers, resulting in a smooth membrane surface with a roughness of 20.1 nm and a low contact angle of 88.3° (Fig. 4). Similar results can be found in the literature where membranes prepared using NMP as solvent had relatively low contact angles (Chang et al., 2017). In the same way, the addition of acetone into PVDF dope solution decreased the surface pore size and contact angles as acetone promoted L-L demixing by decreasing the viscosity of PVDF solution (Fig. 3c, d).

On the other hand, Fig. 3 (e, f) shows that the addition of DBP into polymer solution leads to a dense skin at the shell side of HF membranes. It is assumed that the significant increase in solution viscosity would greatly delay L-L demixing, suggesting that coagulant (water) would diffuse slowly through the dope solution and form smaller pores on shell skin. Despite its dense surface skin, the mean pore sizes of TEPD-1 and TEPD-2 were much higher than the ones of other samples due to its spherulitic structures under the dense shell skin. TEPD-2 obtained the highest surface roughness of 120.0 nm and the contact angle of 117.7° owing to the high surface peaks formed during NIPS process dominated by S-L demixing process. In contrast, the membranes fabricated from dope solutions containing toluene displayed very distinct surface morphology. Fig. 3 (g, h) illustrates that both TEPT-1 and TEPT-2 have more porous skins than the ones observed in other samples. Further increase in the weight ratio of toluene in the dope solution brought about an increase in the surface pore size. Surface roughness and the contact angle of TEPT-2 are the second highest (112.8 nm and 114.2°, respectively) among all the samples. The porous surface layer with improved hydrophobicity is expected to contribute to higher mass transfer rate in MD with TEPT-2.

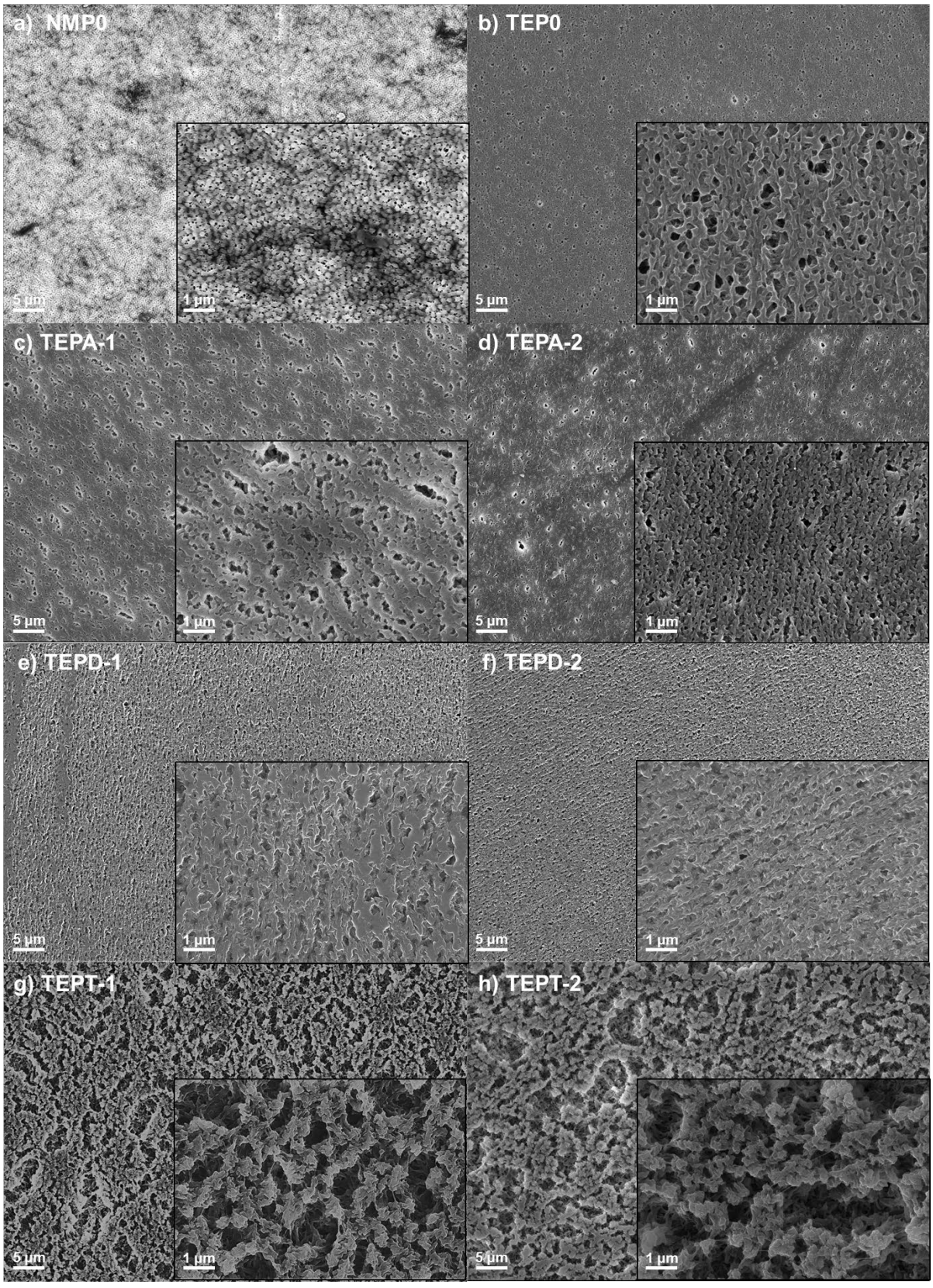


**Fig. 3.** SEM images displaying the surface morphology of hollow fiber membranes cast from 11 wt.% PVDF in (a) NMP; (b) TEP; (c, d) TEP with acetone; (e, f) TEP with DBP; (g, h) TEP with toluene.

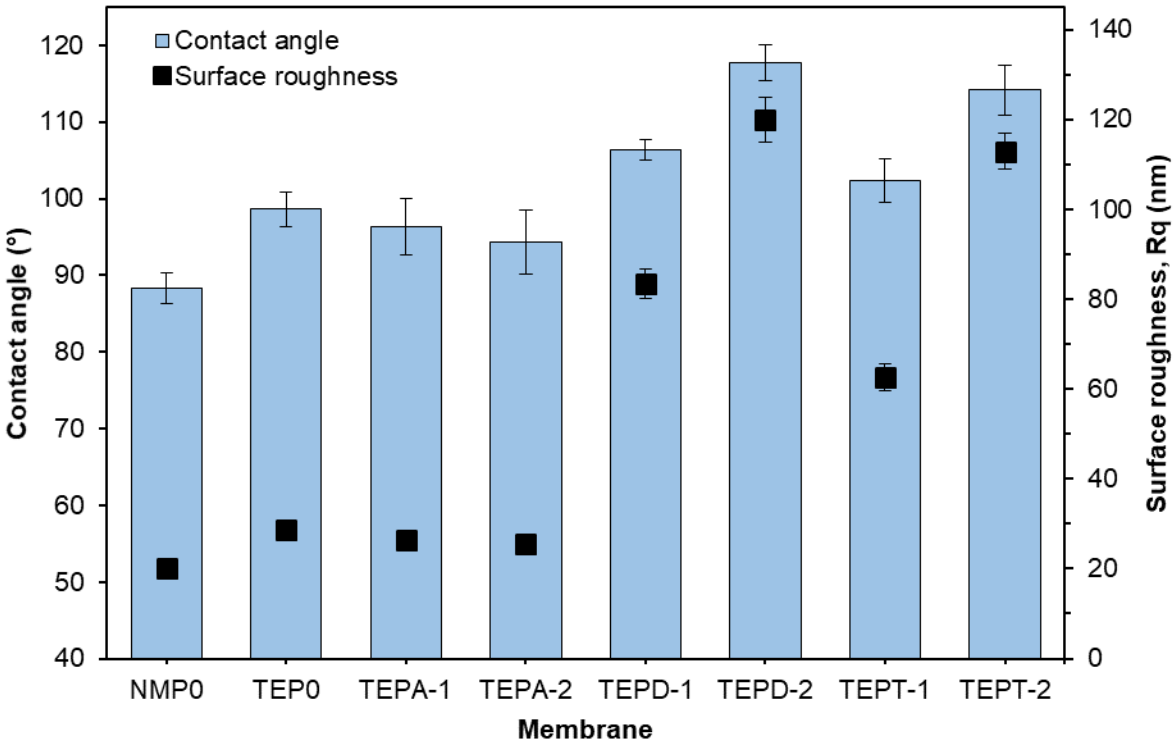


**Fig. 4.** The water contact angles measured on the shell surface of hollow fiber membrane prepared using dope solutions containing various non-solvents.

## 3.5 MD flux performance

### 3.5.1 Comparison of MD performance using various membranes

Fig. 5 shows the flux permeation of different membranes in DCMD. Given that same high salt rejection of 99.99% is observed, the tested HF membrane samples demonstrate various permeation performance as their morphologies and properties are significantly different. TEP0 has higher water flux than NMP0 possibly due to its increased porosity and mean pore size. TEPA-2 had a lower flux than NMP0 although they consisted of similar porosity, mean pore size and contact angles. The increased thickness of TEPA-2 could be the main contributor towards the increased mass transfer resistance that curtain the permeation performance. On the other side, both TEPD-0 and TEPD-1 suffered from rapid wetting within half an hour of starting experiments due to their large pore size; hence, their results are not demonstrated in Fig. 5. TEPT-2 showed a significantly improved flux over TEP0 from 14.9 to 18.9 LMH. The much-improved inner structure with large porosity and mean pore size offset the large thickness of TEPT-2; besides, this membrane had much reduced mass transfer resistance at membrane surface due to its porous skin layer (Fig. 3h). Therefore, TEPT-2 had the highest flux among all tested membrane samples.

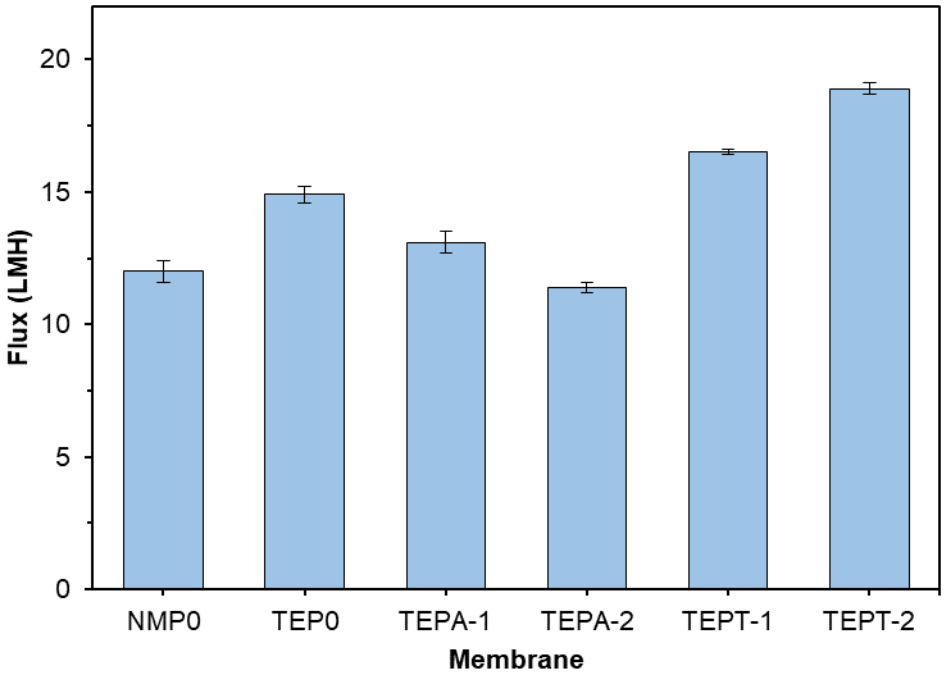


**Fig. 5.** Flux permeation comparison of membrane samples prepared by using dope solutions containing various non-solvents in direct contact membrane distillation

### 3.5.2 Long-term operation of membrane distillation

Fig. 6 presents the flux performances of TEP0, TEPT-2 and the commercial membrane from Econity in the same DCMD configuration for 72 h. The commercial HF membranes demonstrated a stable low flux of 6.4 LMH. In contrast, NMP0 had a higher initial flux but its flux and salt rejection steadily decreased during 72 h operation. The deteriorated permeation performance can be caused by partial pore wetting. On the other hand, TEPT-2 had a high and stable flux of 18.8 LMH for 72 h operation owing to its bicontinuous structure and porous skin morphology. Also, it showed no sign of wetting as it maintained a high salt rejection of 99.99%. The performance test results confirm that the addition of toluene into dope solution produces high-performance HF membranes with improved flux while maintaining high rejection of inorganic salts in the feed.

TEPT-2 shows high permeation performance comparable to those at similar DCMD configurations in the literature. Lu, Zuo, and Chung (2016) developed a super hydrophobic HF PVDF membrane via surface-modification; the membrane had an average flux of 21 LMH at 60 °C feed and 16 °C permeate. Chang et al. (2017) developed a HF membrane with a green solvent, which had an average flux of 20 LMH at 60 °C feed and 15 °C permeate temperature. In this study, a flux of 18.8 LMH was achieved at a higher permeate temperature of 20 °C (same feed temperature). Since this study is focused on the effects of morphology on the improvement of MD performance, the composition of dope solutions and

spinning conditions were not optimized; hence, the thickness of TEPT-2 was higher than those reported in the literature, leading to significantly higher mass transfer resistance. Moreover, TEPT-2 can be further improved via surface modifications, which means that the technique of using toluene as NS into dope solutions is vastly compatible with other modification methods to obtain high-performance HF membranes for MD.

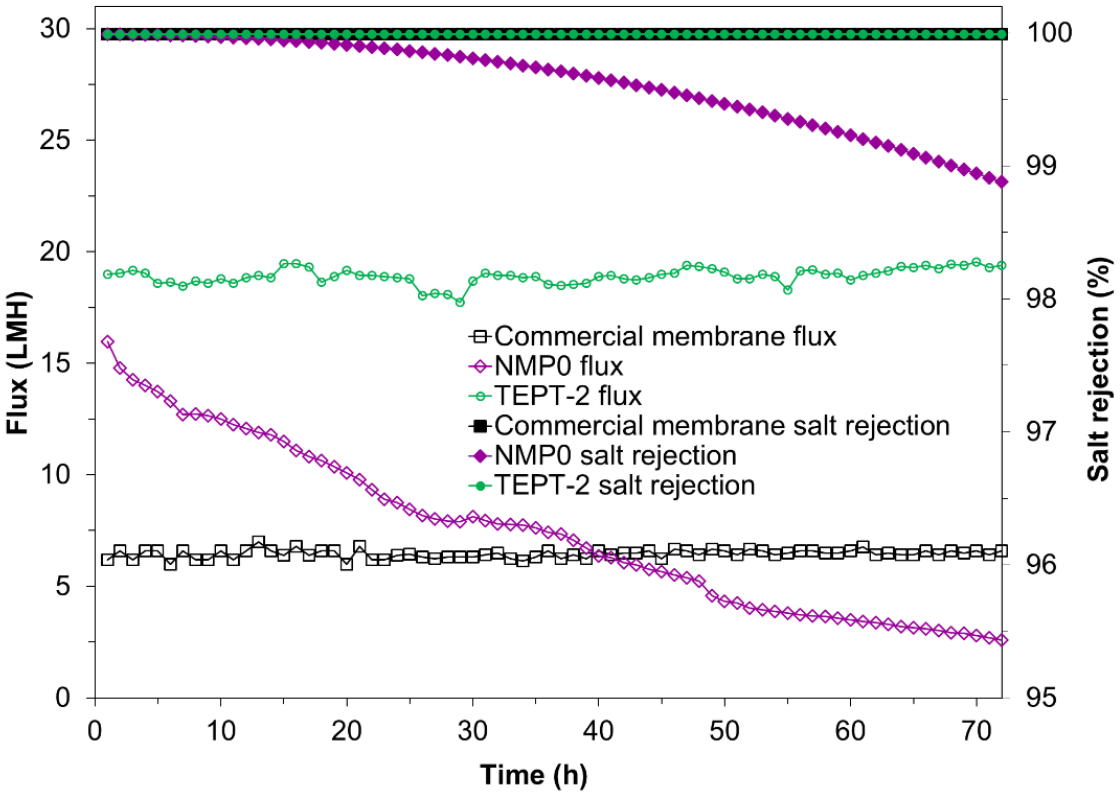


**Fig. 6.** Flux performance of the commercial membrane, NMP0 and TEPT-2

## 4. Conclusions

The effect of various dope solution NSs on the inner structure and surface morphology of hollow fiber membranes was investigated to improve MD performance. The viscosity and water affinity of dope solutions were controlled to manipulate the sequence of L-L and S-L demixing rates of NIPS process to obtain a desirable membrane morphology. Permeation performance of HF membranes in MD was evaluated in association with improvement in membrane morphology and mean pore size. The sequence of L-L and S-L demixing rates between solvent and coagulant in NIPS was determined from the viscosity and water affinity of dope solutions. The mixing of various NSs into the dope solutions resulted in formation of HF membranes with very different morphologies and properties. The results indicated that bicontinuous inner structures with porous shell skins could be achieved by adding toluene into the dope solution. TEPT-2 demonstrated significant improvement in porosity and mean pore size while maintaining mechanical integrity. Using this membrane, a high flux of 18.9 LMH with a salt

rejection of 99.99% was achieved in the DCMD process at 60 °C/20 °C (feed/permeate) when tested for 72 h. In conclusion, this fabrication strategy is compatible with other membrane modification techniques for mass production of HF membranes with high selectivity and permeation performance owing to its low complexity and economic cost.

**Acknowledgment**

This study was funded by the Korea Ministry of Environment (MOE) and Korea Environmental Industry & Technology Institute (KEITI) as "A Industrial Facilities & Infrastructure Research Program" [146667]. The authors also acknowledge the support of the Australian Government Research Training Program Scholarship and the Grant from the ARC Future Fellowship (FT140101208).

**Reference:**

Abed, M. R. M., Kumbharkar, S. C., Groth, A. M., & Li, K. (2012). Ultrafiltration PVDF hollow fibre membranes with interconnected bicontinuous structures produced via a single-step phase inversion technique. *Journal of Membrane Science, 407-408*, 145-154. doi:10.1016/j.memsci.2012.03.029

Ahmad, A. L., Otitoju, T. A., & Ooi, B. S. (2018). Hollow fiber (HF) membrane fabrication: A review on the effects of solution spinning conditions on morphology and performance. *Journal of Industrial and Engineering Chemistry*.

Ahmed, F. E., Lalia, B. S., & Hashaikeh, R. (2015). A review on electrospinning for membrane fabrication: Challenges and applications. *Desalination, 356*, 15-30. doi:https://doi.org/10.1016/j.desal.2014.09.033

Bonyadi, S., & Chung, T.-S. (2009). Highly porous and macrovoid-free PVDF hollow fiber membranes for membrane distillation by a solvent-dope solution co-extrusion approach. *Journal of Membrane Science, 331*(1-2), 66-74. doi:10.1016/j.memsci.2009.01.014

Buonomenna, M. G., Macchi, P., Davoli, M., & Drioli, E. (2007). Poly(vinylidene fluoride) membranes by phase inversion: the role the casting and coagulation conditions play in their morphology, crystalline structure and properties. *European Polymer Journal, 43*(4), 1557-1572. doi:10.1016/j.eurpolymj.2006.12.033

Chang, J., Zuo, J., Zhang, L., O'Brien, G. S., & Chung, T.-S. (2017). Using green solvent, triethyl phosphate (TEP), to fabricate highly porous PVDF hollow fiber membranes for membrane distillation. *Journal of Membrane Science, 539*, 295-304. doi:10.1016/j.memsci.2017.06.002

Deshmukh, A., Boo, C., Karanikola, V., Lin, S., Straub, A. P., Tong, T., . . . Elimelech, M. (2018). Membrane distillation at the water-energy nexus: limits, opportunities, and challenges. *Energy & Environmental Science, 11*(5), 1177-1196. doi:10.1039/c8ee00291f

Eykens, L., De Sitter, K., Dotremont, C., Pinoy, L., & Van der Bruggen, B. (2017). Membrane synthesis for membrane distillation: A review. *Separation and Purification Technology, 182*, 36-51.

475 Franken, A., Nolten, J., Mulder, M., Bargeman, D., & Smolders, C. (1987). Wetting criteria
476 for the applicability of membrane distillation. *Journal of Membrane Science, 33*(3),
477 315-328.
478 García-Payo, M. C., Essalhi, M., & Khayet, M. (2010). Effects of PVDF-HFP concentration
479 on membrane distillation performance and structural morphology of hollow fiber
480 membranes. *Journal of Membrane Science, 347*(1-2), 209-219.
481 doi:10.1016/j.memsci.2009.10.026
482 Hung, W.-L., Wang, D.-M., Lai, J.-Y., & Chou, S.-C. (2016). On the initiation of macrovoids
483 in polymeric membranes – effect of polymer chain entanglement. *Journal of Membrane*
484 *Science, 505*, 70-81. doi:10.1016/j.memsci.2016.01.021
485 Jung, J. T., Wang, H. H., Kim, J. F., Lee, J., Kim, J. S., Drioli, E., & Lee, Y. M. (2018).
486 Tailoring nonsolvent-thermally induced phase separation (N-TIPS) effect using triple
487 spinneret to fabricate high performance PVDF hollow fiber membranes. *Journal of*
488 *Membrane Science, 559*, 117-126. doi:10.1016/j.memsci.2018.04.054
489 Li, Q., Xu, Z.-L., & Yu, L.-Y. (2010). Effects of mixed solvents and PVDF types on
490 performances of PVDF microporous membranes. *Journal of Applied Polymer Science,*
491 *115*(4), 2277-2287. doi:10.1002/app.31324
492 Li, Y., Dong, S., & Zhu, L. (2018). Preparation of novel poly(vinylidene fluoride)/TiO2
493 photocatalysis membranes for use in direct contact membrane distillation. *Journal of*
494 *Nanoparticle Research, 20*(3). doi:10.1007/s11051-018-4167-9
495 Liao, Y., Wang, R., Tian, M., Qiu, C., & Fane, A. G. (2013). Fabrication of polyvinylidene
496 fluoride (PVDF) nanofiber membranes by electro-spinning for direct contact membrane
497 distillation. *Journal of Membrane Science, 425*, 30-39.
498 Lin, D.-J., Chang, C.-L., Chen, T.-C., & Cheng, L.-P. (2002). Microporous PVDF membrane
499 formation by immersion precipitation from water/TEP/PVDF system. *Desalination,*
500 *145*(1), 25-29. doi:https://doi.org/10.1016/S0011-9164(02)00340-5
501 Lin, D.-J., Chang, H.-H., Chen, T.-C., Lee, Y.-C., & Cheng, L.-P. (2006). Formation of porous
502 poly(vinylidene fluoride) membranes with symmetric or asymmetric morphology by
503 immersion precipitation in the water/TEP/PVDF system. *European Polymer Journal,*
504 *42*(7), 1581-1594. doi:10.1016/j.eurpolymj.2006.01.027
505 Lu, K.-J., Zuo, J., & Chung, T.-S. (2016). Tri-bore PVDF hollow fibers with a super-
506 hydrophobic coating for membrane distillation. *Journal of Membrane Science, 514*,
507 165-175.
508 Mansourizadeh, A., & Ismail, A. F. (2011). Preparation and characterization of porous PVDF
509 hollow fiber membranes for CO2 absorption: Effect of different non-solvent additives
510 in the polymer dope. *International Journal of Greenhouse Gas Control, 5*(4), 640-648.
511 doi:10.1016/j.ijggc.2011.03.009
512 McGaughey, A. L., Gustafson, R. D., & Childress, A. E. (2017). Effect of long-term operation
513 on membrane surface characteristics and performance in membrane distillation.
514 *Journal of Membrane Science, 543*, 143-150. doi:10.1016/j.memsci.2017.08.040
515 Munirasu, S., Banat, F., Durrani, A. A., & Haija, M. A. (2017). Intrinsically superhydrophobic
516 PVDF membrane by phase inversion for membrane distillation. *Desalination, 417*, 77-
517 86. doi:10.1016/j.desal.2017.05.019
518 Nejati, S., Boo, C., Osuji, C. O., & Elimelech, M. (2015). Engineering flat sheet microporous
519 PVDF films for membrane distillation. *Journal of Membrane Science, 492*, 355-363.
520 doi:10.1016/j.memsci.2015.05.033
521 Pinnau, I., & Koros, W. J. (1993). A qualitative skin layer formation mechanism for membranes
522 made by dry/wet phase inversion. *Journal of Polymer Science Part B: Polymer Physics,*
523 *31*(4), 419-427.

524 Qiu, H., Peng, Y., Ge, L., Villacorta Hernandez, B., & Zhu, Z. (2018). Pore channel surface
525 modification for enhancing anti-fouling membrane distillation. *Applied Surface Science,*
526 *443*, 217-226. doi:10.1016/j.apsusc.2018.03.004
527 Shi, F., Ma, Y., Ma, J., Wang, P., & Sun, W. (2012). Preparation and characterization of
528 PVDF/TiO2 hybrid membranes with different dosage of nano-TiO2. *Journal of*
529 *Membrane Science, 389*, 522-531. doi:10.1016/j.memsci.2011.11.022
530 Smolders, C., Reuvers, A., Boom, R., & Wienk, I. (1992). Microstructures in phase-inversion
531 membranes. Part 1. Formation of macrovoids. *Journal of Membrane Science, 73*(2-3),
532 259-275.
533 Sukitpaneenit, P., & Chung, T.-S. (2009). Molecular elucidation of morphology and
534 mechanical properties of PVDF hollow fiber membranes from aspects of phase
535 inversion, crystallization and rheology. *Journal of Membrane Science, 340*(1-2), 192-
536 205. doi:10.1016/j.memsci.2009.05.029
537 Tao, M.-m., Liu, F., Ma, B.-r., & Xue, L.-x. (2013). Effect of solvent power on PVDF
538 membrane polymorphism during phase inversion. *Desalination, 316*, 137-145.
539 doi:10.1016/j.desal.2013.02.005
540 Venault, A., Chang, Y., Wu, J.-R., & Wang, D.-M. (2014). Influence of solvent composition
541 and non-solvent activity on the crystalline morphology of PVDF membranes prepared
542 by VIPS process and on their arising mechanical properties. *Journal of the Taiwan*
543 *Institute of Chemical Engineers, 45*(3), 1087-1097. doi:10.1016/j.jtice.2013.08.014
544 Wang, P., Teoh, M. M., & Chung, T. S. (2011). Morphological architecture of dual-layer
545 hollow fiber for membrane distillation with higher desalination performance. *Water Res,*
546 *45*(17), 5489-5500. doi:10.1016/j.watres.2011.08.012
547 Wu, P., Jiang, L. Y., & Hu, B. (2018). Fabrication of novel PVDF/P(VDF-co-HFP) blend
548 hollow fiber membranes for DCMD. *Journal of Membrane Science, 566*, 442-454.
549 doi:https://doi.org/10.1016/j.memsci.2018.09.015
550 Yao, M., Woo, Y. C., Tijing, L. D., Shim, W.-G., Choi, J.-S., Kim, S.-H., & Shon, H. K. (2016).
551 Effect of heat-press conditions on electrospun membranes for desalination by direct
552 contact membrane distillation. *Desalination, 378*, 80-91.
553 doi:https://doi.org/10.1016/j.desal.2015.09.025
554 Yeow, M., Liu, Y., & Li, K. (2003). Isothermal phase diagrams and phase-inversion behavior
555 of poly (vinylidene fluoride)/solvents/additives/water systems. *Journal of Applied*
556 *Polymer Science, 90*(8), 2150-2155.
557 Zhang, H., Li, B., Sun, D., Miao, X., & Gu, Y. (2018). SiO2-PDMS-PVDF hollow fiber
558 membrane with high flux for vacuum membrane distillation. *Desalination, 429*, 33-43.
559 doi:10.1016/j.desal.2017.12.004
560 Zhang, P.-Y., Yang, H., Xu, Z.-L., Wei, Y.-M., Guo, J.-L., & Chen, D.-G. (2013).
561 Characterization and preparation of poly (vinylidene fluoride)(PVDF) microporous
562 membranes with interconnected bicontinuous structures via non-solvent induced phase
563 separation (NIPS). *Journal of Polymer Research, 20*(2), 66.
564 Zhu, J., Jiang, L., & Matsuura, T. (2015). New insights into fabrication of
565 hydrophobic/hydrophilic composite hollow fibers for direct contact membrane
566 distillation. *Chemical Engineering Science, 137*, 79-90. doi:10.1016/j.ces.2015.05.064

567